Environmental Pollution 330 (2023) 121805

Contents lists available at ScienceDirect

Environmental Pollution

journal homepage: www.elsevier.com/locate/envpol

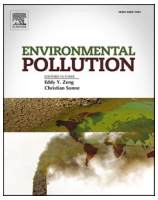

Investigation of four-year chemical composition and organic aerosol sources of submicron particles at the ATOLL site in northern France☆

Hasna Chebaicheb [a,b,c], Joel F. de Brito [a,*], Gang Chen [d,e], Emmanuel Tison [a], Caroline Marchand [b,c], André S.H. Prévôt [d], Olivier Favez [b,c], Véronique Riffault [a,c]

[a] IMT Nord Europe, Institut Mines-Télécom, Université de Lille, Centre for Energy and Environment, 59000, Lille, France
[b] Institut National de l'environnement Industriel et des Risques (INERIS), 60550, Verneuil-en-Halatte, France
[c] Laboratoire Central de Surveillance de la Qualité de l'Air (LCSQA), 60550, Verneuil-en-Halatte, France
[d] Laboratory of Atmospheric Chemistry, Paul Scherrer Institute, 5232, Villigen, Switzerland
[e] MRC Centre for Environment and Health, Environmental Research Group, Imperial College London, London, W120BZ, UK

ARTICLE INFO

Keywords:
Air quality
Urban pollution
Source apportionment
Rolling PMF
Particulate matter
ATOLL platform

ABSTRACT

This study presents the first long-term online measurements of submicron (PM_1) particles at the ATOLL (ATmospheric Observations in liLLe) platform, in northern France. The ongoing measurements using an Aerosol Chemical Speciation Monitor (ACSM) started at the end of 2016 and the analysis presented here spans through December 2020. At this site, the mean PM_1 concentration is 10.6 μg m^{-3}, dominated by organic aerosols (OA, 42.3%) and followed by nitrate (28.9%), ammonium (12.3%), sulfate (8.6%), and black carbon (BC, 8.0%). Large seasonal variations of PM_1 concentrations are observed, with high concentrations during cold seasons, associated with pollution episodes (e.g. over 100 μg m^{-3} in January 2017). To study OA origins over this multiannual dataset we performed source apportionment analysis using rolling positive matrix factorization (PMF), yielding two primary OA factors, a traffic-related hydrocarbon-like OA (HOA) and biomass-burning OA (BBOA), and two oxygenated OA (OOA) factors. HOA showed a homogeneous contribution to OA throughout the seasons (11.8%), while BBOA varied from 8.1% (summer) to 18.5% (winter), the latter associated with residential wood combustion. The OOA factors were distinguished between their less and more oxidized fractions (LO-OOA and MO-OOA, on average contributing 32% and 42%, respectively). During winter, LO-OOA is identified as aged biomass burning, so at least half of OA is associated with wood combustion during this season. Furthermore, ammonium nitrate is also a predominant aerosol component during cold-weather pollution episodes – associated with fertilizer usage and traffic emissions. This study provides a comprehensive analysis of submicron aerosol sources at the recently established ATOLL site in northern France from multiannual observations, depicting a complex interaction between anthropogenic and natural sources, leading to different mechanisms of air quality degradation in the region across different seasons.

1. Introduction

Air pollution remains a major environmental risk to humans, with fine particles $PM_{2.5}$ (Particulate matter with an aerodynamic diameter smaller than 2.5 μm) leading to cardiovascular and respiratory diseases and premature mortality (Kelly and Fussell, 2015). In Europe, more than 307 000 premature deaths have been attributed to fine particle exposure (Air quality in Europe, 2021). The north of France, in particular, is affected by relatively high PM concentrations, frequently exceeding the annual $PM_{2.5}$ concentration of 5 μg m^{-3} recommended by the WHO (WHO Air Quality Guidelines, 2021). The Hauts-de-France region is the 2nd most densely populated area in France with 6 million inhabitants. It is affected by intense traffic, residential, industrial, and agricultural emissions combined with transboundary pollution from nearby countries such as the United Kingdom, Belgium, the Netherlands, and Germany, making it an air pollution hotspot (Roig Rodelas et al., 2019; Thunis et al., 2021; Potier et al., 2019; Waked et al., 2014, 2018). While tighter emission controls are expected to decrease PM concentrations (e.

☆ This paper has been recommended for acceptance by Admir Créso Targino.

* Corresponding author.
E-mail address: joel.brito@imt-nord-europe.fr (J. F. de Brito).

https://doi.org/10.1016/j.envpol.2023.121805
Received 24 February 2023; Received in revised form 8 May 2023; Accepted 9 May 2023
Available online 10 May 2023

g., ban of new combustion engine vehicles by 2035 throughout the EU), quantifying the efficiency of mitigation strategies requires an in-depth understanding of current sources. This is particularly relevant when focusing on the finer aerosol fraction such as submicron particles (PM_1), which can be strongly affected by secondary formation (Pandis et al., 2016). Most notably, organic aerosols (OA), formed from a complex pool of compounds, are one of the dominant submicron aerosol species in Central Europe (Chen et al., 2022). For instance, in northern France, the OA and nitrates have been shown to dominate the non-refractory PM_1 (NR-PM_1) at background sites, whereas sulfate and nitrate were the most dominant species in summer at the industrial and coastal sites (Crenn et al., 2017, Zhang et al., 2021). Sulfate was also observed to be a major species during summertime in Marseille, in the south of France, attributed to the influence of local industrial activities and shipping (Chazeau et al., 2021).

The study of OA sources in recent years has largely been conducted using Positive Matrix Factorization (PMF, Paatero and Tapper, 1994) on Aerosol Mass Spectrometers (Allan et al., 2003), or its compact version, termed Aerosol Chemical Speciation Monitor (ACSM, Ng et al., 2011b). The PMF analysis of those observations has drastically improved our knowledge of key sources of OA in Europe over the past two decades (e.g. Crippa et al., 2014). Recently, Roig Rodelas et al. (2019) investigated the OA sources during a five-week wintertime field campaign in Douai, 30 km south of Lille, highlighting the significant contribution of oxygenated organic aerosols to the site, and the impact of air masses coming from Eastern Europe. Similarly, at an urban background site in Barcelona (Spain), both Oxygenated OA (OOA) fractions dominate the OA total mass over the two one-year study periods (Via et al., 2021), increased by air masses coming from inland Europe and the Mediterranean, especially the more oxidized OOA.

Whereas the PMF analysis applied on multiannual ACSM datasets hitherto yielded important results, notably allowing the identification of primary versus secondary OA (POA and SOA, respectively) sources across multiple seasons, the inherent limitation of fixed factors on traditional PMF method forces longer datasets to be split, typically into three months sub-sets (e.g. Canonaco et al., 2015; Zhang et al., 2019). This method has the drawback of requiring multiple independent PMF analyses, being labor-intensive, and prone to discrepancies between individual runs. Recently a rolling PMF method has been developed (Canonaco et al., 2021; Parworth et al., 2015; Chen et al., 2022), allowing the study of long-term datasets in a single iteration via a sliding time window, thus enabling inter and intra-seasonal variations of OA source profiles. The recently developed method has already been applied at several sites across Europe, although limited to one-year datasets (Atabakhsh et al., 2023; Canonaco et al., 2021; Chazeau et al., 2021; Chen et al., 2021; Tobler et al., 2021; Zografou et al., 2022).

In this context, we have studied PM_1 composition and OA sources since 2016 at a suburban site in Lille, known as the ATOLL (ATmospheric Observations in liLLe) platform. Recent studies at this site have shown a dominating effect of ammonium nitrate and organics on the aerosol optical properties (Velazquez-Garcia et al., 2023), as well as intense gas-to-particle conversion during spring and summer (Crumeyrolle et al., 2023). Thus, the objectives of this study are i) to apply for the first time the rolling PMF method on a multiannual dataset of organic aerosol at this site, and ii) to better understand PM_1 sources at the ATOLL platform. The results aim at better understanding aerosol sources via long-term analysis and quantify their contribution in the North-Western European region, therefore supporting the development of effective emission reduction strategies.

2. Methodology

2.1. Site description

The ATOLL platform (70 m a.s.l; 50.61° N; 3.14° E) is considered a suburban site, located on the rooftop of the University of Lille building in Villeneuve d'Ascq, within the Lille metropolitan area, one of the most densely populated areas in France. ATOLL is located roughly 4 km southeast of downtown Lille (Fig. S1). Furthermore, the region is located at the crossroads of transnational pollution transport including Belgium, Germany, the Netherlands, and the UK. This platform contributes to the French CARA program (Favez et al., 2021) and is a French National Facility of the European Aerosols, Clouds and Trace gases Research InfraStructure (ACTRIS), following the corresponding inlet setup and instrumentation deployment guidelines (https://www.actris-ecac.eu/measurement-guidelines.html). The period considered in this study lasts from October 2016 to December 2020 with some data gaps mostly due to instrument maintenance, calibrations, and temporary relocation for intensive field campaigns.

2.2. Instrumentation

The Quadrupole ACSM (Q-ACSM, Aerodyne Research Inc., USA) is based on aerosol mass spectrometery technology where ambient particles are sampled and the submicron fraction is focused by an aerodynamic lens onto a vaporizer heated at 600 °C after being pumped through a vacuum chamber. The vaporized compounds are ionized and fragmented by electron ionization at 70 eV, then detected with a quadrupole mass spectrometer (measurement range 0–200 amus). The analysis of the fragments allows reconstruction of their chemical composition, notably OA, sulfate (SO_4), nitrate (NO_3), ammonium (NH_4), and chloride (Cl) with a time resolution of 30 min and detection limits ranging from 0.01 to 0.28 μg m^{-3} for the different species (Ng et al., 2011a). The Cl contribution was negligible and is not addressed here.

The Q-ACSM sampling line (OD = 9.5 mm; ID = 6.5 mm; 2.3-m-long stainless tube; flow: 3 L min^{-1}) is equipped with a $PM_{2.5}$ cyclone (URG-2000-30EQ, URG Corp., USA) and a Nafion dryer to maintain relative humidity at the instrument entrance below 40%, which reduces artifacts from bouncing effects. ACSM chemical calibration is performed by injecting size-selected (typically 300 nm) ammonium nitrate and ammonium sulfate particles. This procedure allows for determining the response factor (RF) of NO_3 and the relative ionization efficiencies (RIE) of NH_4 and SO_4. The RF and RIE calibrations (summarized in Table S2) are stable and typically applied yearly Table S2. To obtain quantitative mass concentrations for ACSM species, a composition-dependent collection efficiency (CDCE) is applied to account for the incomplete detection of aerosol species (Middlebrook et al., 2012) (Fig. S3).

Ancillary measurements for this analysis include a 7-wavelength Aethalometer (AE33, Magee Scientific, USA). This instrument measures the optical attenuation and converts it into aerosol light absorption for each wavelength with a time resolution of 1 min (Drinovec et al., 2015). Ambient black carbon (BC) equivalent concentrations are derived at 880 nm, using the manufacturer's mass absorption efficiency (MAE) at this wavelength (7.77 m^2 g^{-1}), following ACTRIS guidelines. The AE33 sampling line (OD = 9.5 mm; ID = 6.5 mm; 2.6-m-long stainless tube and 1.85 m static dissipative tubing; flow: 5 L min^{-1}) is equipped with a PM_1 cyclone (BGI SCC1.197, Mesa Labs, USA). A Nafion dryer was installed in summer 2020 just before the dissipative tubing.

Meteorological variables (temperature, relative humidity, wind speed and direction) were collected from a weather station (Vantage Pro, DAVIS Inc, USA) collocated with the instruments. Temperature and relative humidity were measured every minute, while the wind direction and speed were obtained using an anemometer with a time stamp of 5 min. $PM_{2.5}$ measurements and nitrogen oxides ($NO + NO_2 = NO_x$) data were obtained from the air quality monitoring network ATMO HdF (at the Lille Fives station, 4.5 km from our site).

2.3. Wind analysis and back-trajectories for cluster calculations

Pollution roses and the diel plots by wind sectors are plotted considering the median concentrations using MATLAB. A wind speed

threshold above 0.3 m s^{-1} was imposed for these plots and analyzed over 22.5° wind sectors. We used the back-trajectories within the NOAA Hybrid Single Particle Lagrangian Integrated Trajectory (HYSPLIT; Draxler, 1999) model using 1° × 1° resolution Global Data Assimilation System (GDAS) files. The back-trajectories were ending at ATOLL from 2016 to 2019 for an arrival altitude of half the planetary boundary layer height at 1-h intervals, 72 h back in time. 4750 back-trajectories were clustered every 6 h using the HYSPLIT model. The method used for clustering analysis is based on the relative variation of the total spatial variance (TSV). The spatial variance is calculated as the sum of the squared distances between the endpoints of the trajectories and the mean of the trajectories in that cluster. The process continues until the last two clusters are combined, and the final number of clusters is determined by identifying the point where the total spatial variance increases rapidly.

2.4. Black Carbon source apportionment

The Aethalometer data are used to further separate BC into fossil fuel (BC_{ff}) and wood burning (BC_{wb}) as proposed by Sandradewi et al. (2008). The method is based on the assumption that wood combustion shows a pronounced absorption in the UV (i.e. high Absorption Angstrom Exponent, AAE) compared to fossil fuel (low AAE). At the ATOLL platform, BC_{ff} and BC_{wb} were separated using the AE33 manufacturer values of $AAE_{ff} = 1$ and $AEE_{wb} = 2$, using the absorption at 470 and 950 nm (Drinovec et al., 2015).

2.5. Source apportionment: the rolling PMF method

The PMF method assumes that concentrations measured at a receptor site can be explained as the linear product of a source matrix (F) and a contributing matrix (G), plus a residual matrix (E) that represents the non-modeled data, as in Eq. (1):

$$X = F.G + E, \tag{1}$$

The two matrices F and G are obtained by an interactive square minimization algorithm that iteratively minimizes the quantity Q which represents the total sum of the squares of the residuals of the model e_{ij} weighted by the measurement uncertainty σ_{ij} for all points ij.

$$Q = \sum_{i=1}^{n} \sum_{j=1}^{m} \left(\frac{e_{ij}}{\sigma_{ij}} \right)^2, \tag{2}$$

The application of PMF is subject to rotational ambiguity in which different combinations of G and F produce similar Q-values, some of which may contain mixed factors and/or unreasonable environmental descriptions of the data. If a priori source chemical information is known, the a-value approach allows overcoming this issue by constraining the expected factor profiles or time series using ME-2 according to Eq. (3) and Eq. (4):

$$f_{solution} = f_{reference} \ (1 \pm a), \tag{3}$$

$$g_{solution} = g_{reference} \ (1 \pm a), \tag{4}$$

This implies that an a-value of 0.1 allows each variable of a mass spectrum to vary by ±10% compared to the reference spectrum. Furthermore, to identify stable PMF solutions and estimate the statistical uncertainty of the analysis, the bootstrap technique is used. It allows a resampling of the original data, i.e. making sub-samples and checking that with these samples we can reach the same solutions and the same contributions of the factors as previously identified (Efron, 1979).

To perform a multi-annual analysis, standard PMF is first performed by seasons in a reference year to (i) determine the number of expected factors throughout the database and (ii) retrieve reference spectra. Afterward, a rolling PMF is applied combining spectra constraints on the primary factors and bootstrapping. The rolling method consists of breaking down the database into shorter periods (e.g. one-month windows, shifting by seven days), having the advantage of allowing some variability in the factor profiles throughout the observation period, across seasons and years.

The standard PMF analysis was performed on the reference year from October 2016 to August 2017, broken down by seasons (Autumn - September, October, November, SON; Winter - December, January, February, DJF; Spring - March, April, May, MAM; and Summer - June, July, August, JJA). This analysis allowed identifying four factors at ATOLL, namely HOA (Hydrocarbon-like OA) related to road traffic, BBOA (Biomass Burning OA) related to biomass combustion, and two OOA factors, including a Less-Oxidized OOA (LO-OOA) and a More-Oxidized one (MO-OOA). At the end of this standard analysis, the primary factor profiles, HOA and BBOA, were extracted from the winter bootstrap PMF solution to be used as a priori information for the rolling PMF analysis (further details are given in the SI, section S2). An initial one-year (2016–2017) rolling PMF analysis has been performed using a 14-day window and one-day step, which was integrated in a multi-site rolling PMF study (Chen et al., 2022), with a suggested criteria list and standardized protocol for this method.

Based on the results of the one-year analysis, rolling PMF was then conducted for the full dataset (October 2016 through December 2020) presented here, using the same reference spectra for the primary factors (HOA and BBOA), however with 28-day windows and seven-day shifting for increased computational efficiency. Section S3 of the SI shows comparable results of the rolling PMF time windows (14-day, shifting by one day vs. 28-day shifting by seven days). Bootstrap was performed with 50 PMF iterations of the rolling window, representing a total of 11 050 different PMF analyses for this four-year dataset. Using the selection criteria defined in Section S3, the best PMF solutions were chosen and then averaged. Rolling PMF was conducted using SoFi Pro software V8.0.6.0 (Source Finder Professional, Datalystica Ltd., Switzerland) with the ME-2 solver in the Igor Pro software environment (Igor Pro version 8.04, Wave Metrics, Inc., USA).

3. Results and discussion

3.1. Temporal variations of PM

Fig. 1 shows the monthly and overall averaged composition of PM_1 species at the ATOLL site for the observation period. The mean concentration of PM_1 for the period is 10.6 μg m^{-3}, with species seasonal concentrations depicted in Table S1. OA is the most abundant component with 41.8% of the total, followed by NO_3, NH_4, SO_4, BC_{ff}, and BC_{wb}, contributing 28.9%, 12.3%, 8.6%, 5.7%, and 2.3%, respectively. The contribution of OA to PM_1 falls within the range of other European urban sites (between 21 and 75%, Chen et al., 2022). The second most abundant species, NO_3, is also significant in PM_1 at other sites in Central Europe such as London, Paris, and at the Cabauw site in the Netherlands (Chen et al., 2022; Zhang et al., 2019; Schlag et al., 2016). Furthermore, Bressi et al. (2021) showed a higher contribution of NO_3 and a lower contribution of SO_4 for regional background sites in Central Europe compared to sites in Northern or Southern Europe.

Monthly mean PM_1 ranges from 3.5 to 20.6 μg m^{-3}, with higher values in winter, with hourly data showing peaks exceeding 80 μg m^{-3}, associated with either organics or inorganic species (Fig. S2). OA, the most abundant component of PM_1, has monthly mean values ranging from 1 to 8 μg m^{-3}, exhibiting higher concentrations in the cold months. NO_3, however, has a specific variability, displaying higher means in spring, associated with heightened ammonia (NH_3) from agricultural activities, and NOx from traffic coupled with favorable photochemical and low-temperature conditions for ammonium nitrate (AN; NH_4NO_3) formation (Bressi et al., 2021; Hendriks et al., 2016). Conversely, SO_4 and BC are fairly consistent, with monthly concentrations around 2 and 3 μg m^{-3}. To deconvolve the sources and processes influencing aerosol composition at the ATOLL site, multiannual rolling PMF was conducted

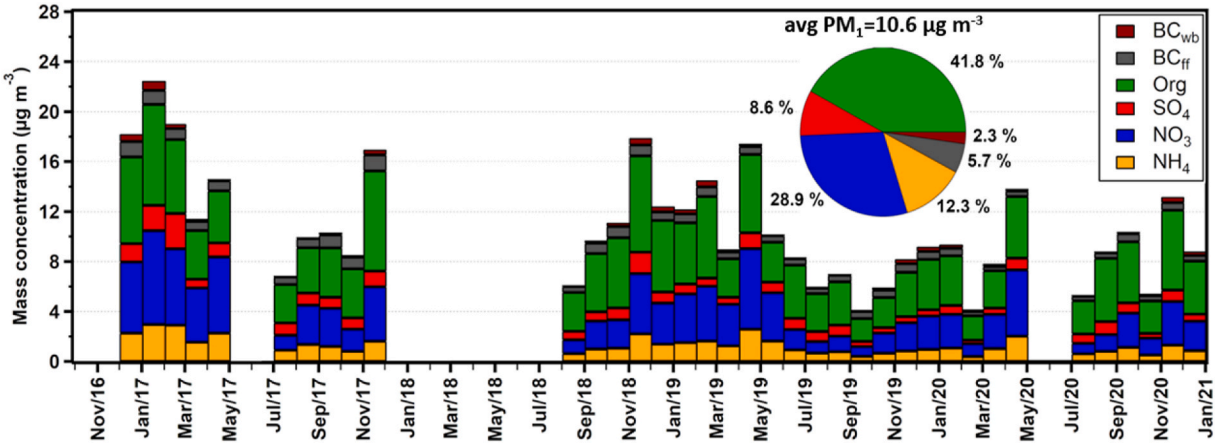

Fig. 1. Monthly means of PM_1 species at the ATOLL site.

on the OA spectra and is presented in the next section. The daily variation of inorganics and OA factors is presented in section 3.3.1.

3.2. Rolling PMF analysis: OA source apportionment

The mean OA factor profiles are presented in Fig. 2. The grey bars indicate the variability of each *m/z* of a factor compared to the reference factors described in section 2.5. The two primary factors HOA and BBOA are constrained with a mean a-value of 0.199 and 0.2, respectively, whereas oxygenated factors were left unconstrained, and were sorted during the analysis via the contribution of the m/z 44 fragment (CO_2^+). Typically, the HOA profile presents characteristic peaks at m/z 43, m/z 57 but also at m/z 41 and m/z 55, corresponding to alkyl and alkenyl fragments. The BBOA profile is characterized by a high contribution of the ions m/z 60 and m/z 73, tracers of biomass-burning combustion. MO-OOA is more oxidized than LO-OOA and presents a strong peak at m/z 44, whereas LO-OOA showed high variability in m/z 43 and 44 and also exhibits the influence of other ions i.e. m/z 29, 55, which is consistent with the mass spectra of other studies (Chen et al., 2021; Tobler et al., 2021; Zhang et al., 2019).

The monthly means of the PMF factors are shown in Fig. 3. The LO-OOA and MO-OOA factors are dominating with 31.9% and 42.3% of OA, respectively, followed by BBOA (14.0%) and HOA (11.8%). As expected, there is a clear seasonality for BBOA with higher concentrations during the cold months, associated with the use of wood for residential heating. Unlike BBOA, HOA is less variable throughout the whole period but with sporadic peaks (Fig. S7) that tend to be associated with BC_{ff}. The HOA factor and BC_{ff} present a correlation across different seasons of $r^2 = 0.48$ (Fig. S9). Indeed, the HOA factor varies from 9.8 % to 12.1% (Fig. S8), consistent with values obtained at other urban European sites (from 7.4% to 12.7%), whereas BBOA in wintertime reaches 18.5%, also comparable to other European sites for the season (8.5%–25.3%) as described in Chen et al. (2022). The MO-OOA factor shows generally a fairly good correlation with secondary inorganic aerosols (NO_3, SO_4, NH_4) across all seasons, and focusing on wintertime only (Figs. S9 and S10, respectively), being likely driven by meteorological conditions and long-range transport, without a clear source identification here.

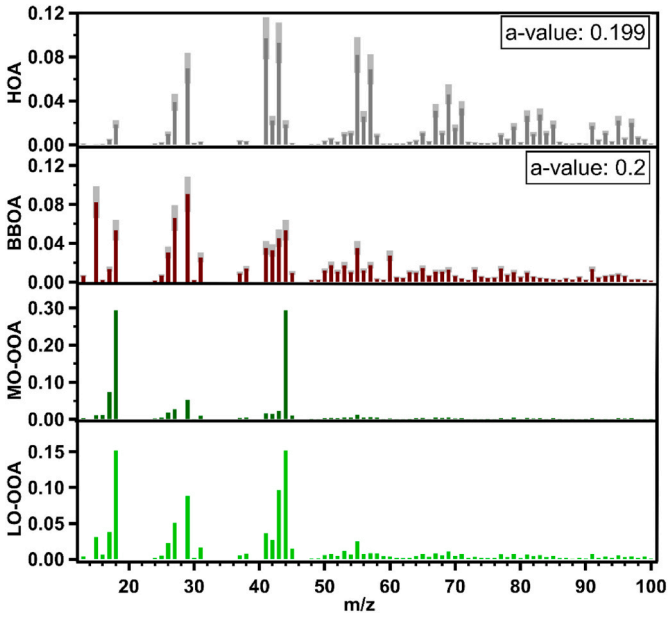

Fig. 2. Mass spectra of OA factors retrieved in the rolling PMF at the ATOLL site.

The LO-OOA factor could be related to different sources during the cold and warm seasons. During wintertime, LO-OOA is associated with aged BBOA, based on the correlation of LO-OOA with BC_{wb} ($r^2 = 0.60$), and BBOA ($r^2 = 0.63$), both shown in Fig. S10, as well as the presence in this factor of m/z 60 in wintertime compared to summertime (Fig. S11). Therefore, at the ATOLL site, the LO-OOA factor is associated with aged residential heating in wintertime, recently identified as a key source of oxidative potential in fine aerosol in Europe, and thus a potential source of deleterious health effects (Daellenbach et al., 2020). Furthermore, BBOA and LO-OOA in wintertime reach a mean contribution of wood combustion (fresh and aged) to OA of 50.4%. In summertime, LO-OOA also contributes to OA (34.0%; Fig. S8) and exhibits an increased m/z 43 and a decreased m/z 44 during warmer months (Fig. S11). Thus it tends to be associated with biogenic SOA following the analysis from Chen et al. (2022) and also depicting a clear trend of increasing LO-OOA with increasing afternoon temperatures in summertime (Fig. S12) (Zhang et al., 2019). Furthermore, summertime spectra of MO-OOA and LO-OOA have been further explored following the *f82* (i.e., m/z 82 ($C_5H_6O^+$)/OA) vs. *f44* plot as proposed by Hu et al. (2015), to verify the potential impact of isoprene epoxydiols (IEPOX) derived SOA. Whereas MO-OOA does not present any IEPOX-SOA signature, with very low *f82* concentrations (3‰), summertime LO-OOA depicts a trend of increasing *f82* with decreasing *f44* (Fig. S13), suggesting a potential role of IEPOX-SOA at this site. Nonetheless, the values of *f82* here for LO-OOA (<8‰) are below those of IEPOX-SOA dominated factors (10–40‰) proposed by Hu et al. (2015). New Particle Formation (NPF) events have additionally been frequently observed at ATOLL by Crumeyrolle et al. (2023) in spring and summer, also supporting strong gas-to-particle conversion in this period. Nevertheless, other processes (non-IEPOX isoprene SOA, monoterpene SOA, aromatics, etc.) could also be relevant for the LO-OOA factor during summertime, but cannot be determined

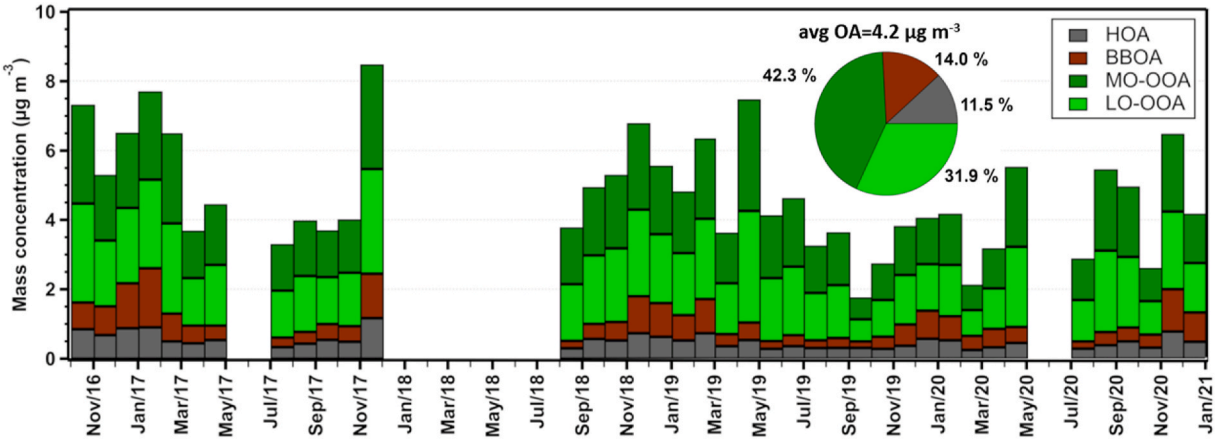

Fig. 3. Monthly averaged OA factor loadings and relative contributions to the total OA at ATOLL.

here.

Fig. 4 presents the mass fraction of aerosol species and OA factors as a function of total PM_1 for different seasons. The black circles show the PM_1 concentrations for each percentile (10–100%). In winter, the 10% highest PM_1 level nearly reaches 30 µg m^{-3}, in contrast with summer (15 µg m^{-3}), and spring and autumn with intermediate values. For winter, spring, and autumn, PM_1 values above the 30th percentile (roughly 5 µg m^{-3}) show an increasing dominance of NO_3 with PM_1 and fairly stable contributions of SO_4 and OA, albeit with a larger fraction being OOA factors. Therefore, as presented previously, NO_3 also plays a major role during pollution events for these colder periods, in agreement with observations at other Central European sites (Bressi et al., 2021; Petit et al., 2015). In summer PM_1 loadings are typically half of those observed in winter, and the composition during pollution episodes depict a different trend compared to other seasons. The SO_4 relative contribution decreases with increasing PM_1, thus not being significant during pollution events. Those, however, are driven by an increasing contribution of OOA fractions, and to a lesser extent, of NO_3. As discussed previously, summertime LO-OOA is particularly associated with biogenic SOA, a potential mechanism for pollution events during that season. It is interesting to note that BC_{ff} has a high contribution under the clean periods, potentially associated with northerly air masses impacted by shipping emissions from the Channel and the North Sea, which is further discussed in subsequent sections.

3.3. Geographic origins of aerosol species

3.3.1. Diel plots according to wind sectors

Diel profiles of aerosol concentrations according to the wind sectors for winter and summer, with contrasting meteorological conditions and aerosol sources, are presented in Figs. 5 and 6, whereas spring and autumn ones can be found in the SI, Figs. S15 and S16. Interestingly, most species present the highest concentrations when ATOLL is influenced by S, SE, E, and NE wind sectors for both seasons, but not when under the influence of the Lille city center (NW–N). It is important to note that wind sectors leading to maximum concentrations such as SE-

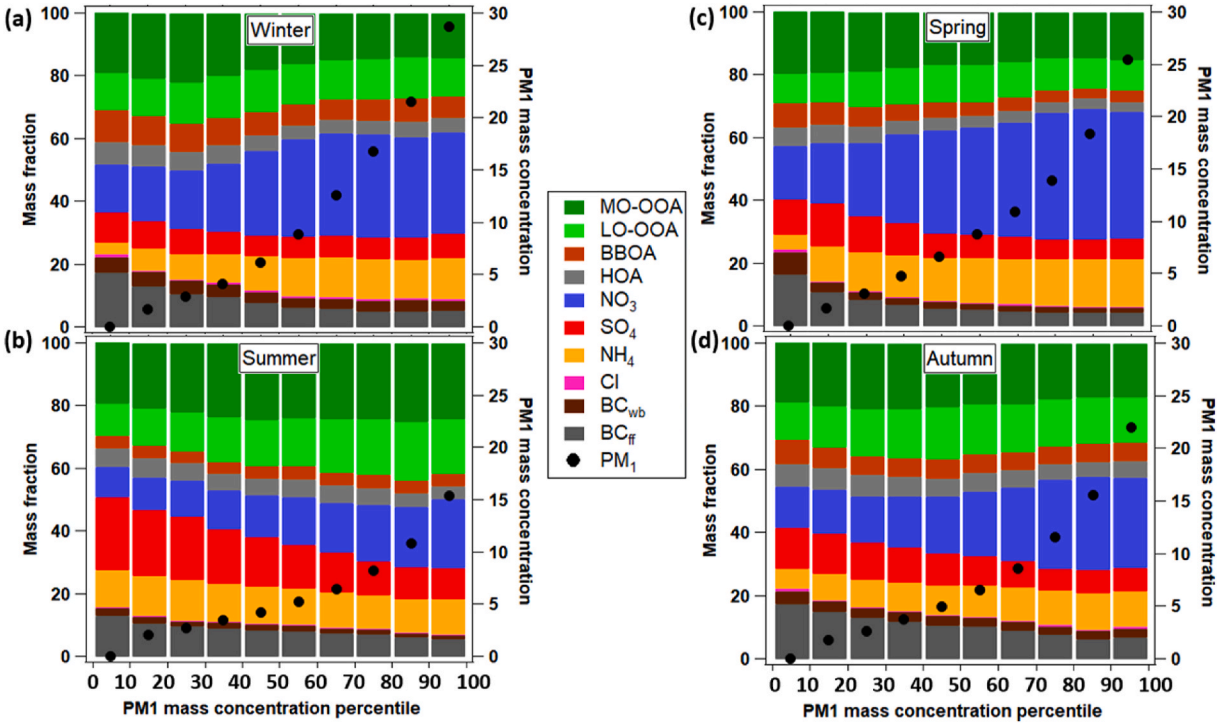

Fig. 4. Seasonal mass fraction of PM_1 species as a function of total PM_1 mass concentration, in a) winter, b) summer, c) spring, and d) autumn.

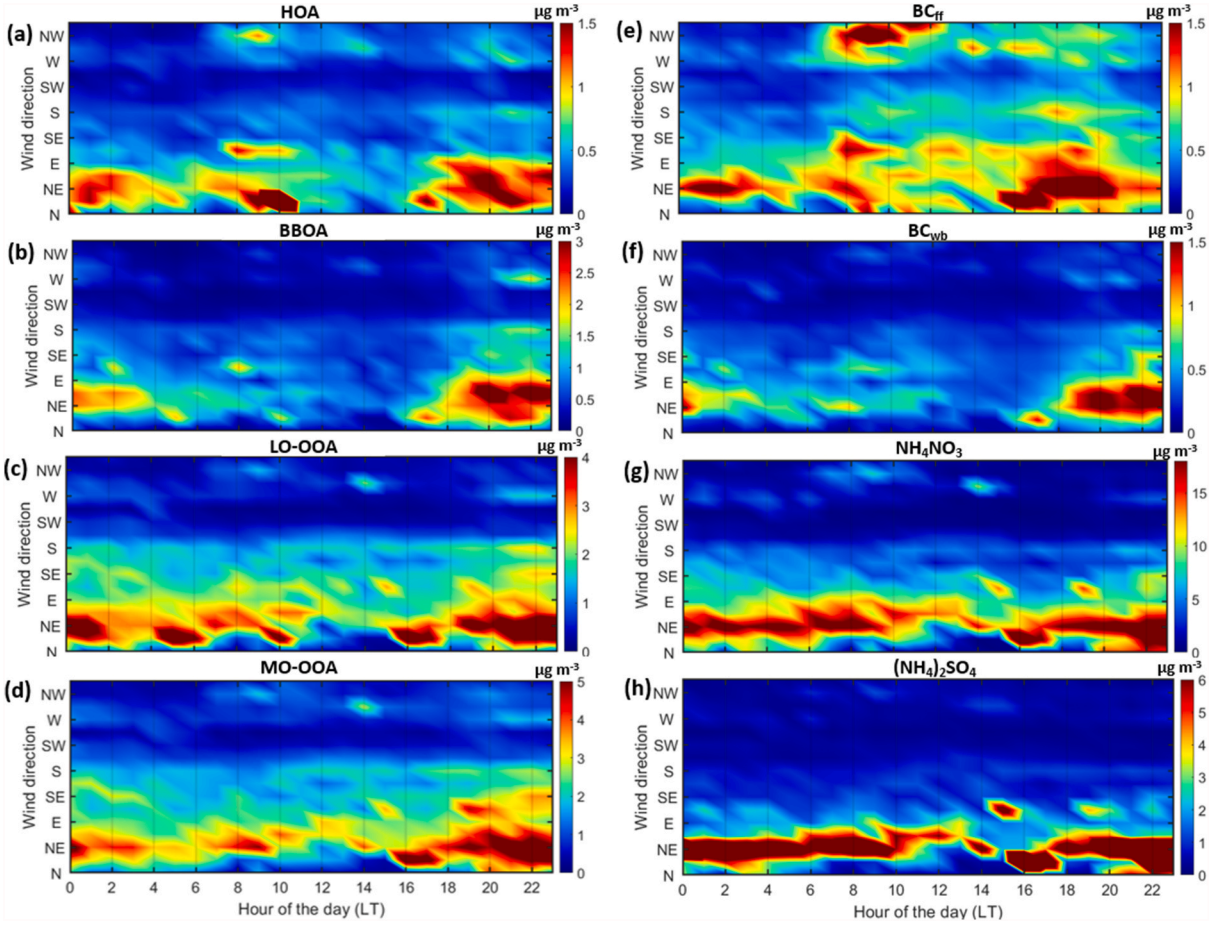

Fig. 5. Diel plots according to wind sectors during the wintertime for a) HOA, b) BBOA, c) LO-OOA, d) MO-OOA, e) BCff, f) BCwb, g) NH4NO3, and h) (NH4)2SO4. The Lille city center is located NW of the ATOLL site. The max value of the color scale represents the 90th percentile. (For interpretation of the references to color in this figure legend, the reader is referred to the Web version of this article.)

NE are prone to reduced wind speeds and pollution build-up conditions (Figs. S14 and S17). In winter, BC_{ff} is the only species that depict a comparable level across all directions, as the sampling site is surrounded by several major roads and highways, thus following fairly well-defined morning and evening rush hour peaks. The diel profile of HOA is generally similar to BC_{ff}, and BC_{wb} with BBOA, due to increased residential heating in the evening, mostly associated with the NE direction (Fig. 5). Considering all wind sectors, the rush hour peaks of HOA across seasons are identifiable, as well as the nighttime peak of BBOA during the colder months (Fig. S20), and the influence of stagnant conditions on the build-up of those primary components (Fig. S18). Both OOA factors follow comparable diel variability and show a similar cycle, with increased, and fairly constant loadings over the NE direction. For MO-OOA, the concentrations increase in the evening, suggesting an effect of the shallower boundary layer height which favors the accumulation of pollutants, in addition to its global regional feature. Furthermore, LO-OOA, follows roughly peak periods of BBOA and BC_{wb} in cold seasons, supporting the influence of biomass burning on this factor. The secondary inorganics, ammonium nitrate and ammonium sulfate, show small diel variability and strong enhancement in the NE sector, indicating a regional origin.

In summer, the diel profiles of HOA and BC_{ff} are less pronounced during the day than during wintertime, being related to the higher boundary layer variability under stronger temperature variations. Wood combustion-related aerosols, BBOA and BC_{wb}, present significantly lower concentrations than in winter, as expected, without a clear trend during the day. The MO-OOA factor depicts an increasing trend during the daytime, whereas LO-OOA has a fairly flat diel profile. Ammonium nitrate shows higher concentrations overnight till around 09:00 mostly from NW, N, and NE directions, followed by a strong decrease, likely caused by volatilization due to higher ambient air temperatures. Conversely, ammonium sulfate exhibits an enhancement in the afternoon. Such behaviors of inorganics have been previously described by Roig Rodelas et al. (2019), in a site 30 km south of ATOLL. During this study, they found correlated enhancement of SO_2 and SO_4, thus pointing towards the advection of sulfur-rich air masses towards the site, in contrast to the local formation of ammonium sulfate. The long-range transport of air masses associated with those higher concentrations is analyzed in more detail in the following section.

3.3.2. *Back-trajectory clustering results*

From the 4750 calculated back-trajectories, we derived six clusters shown in Fig. 7a (detailed in Fig. S21): C1 (southwest), C2 (local), C3 (south), C4 (north), C5 (east), C6 (northwest). Clusters C4 (6% of occurrence) and C6 (10%) from north and northwest are influenced mainly by marine air masses, but also potentially by the UK. Cluster C1 with 23% of occurrence, is affected also by oceanic air masses and contains a continental component (northern France). Cluster C2, the most frequent (37%), is more local and presents at the same time as the marine and continental air masses. Finally, clusters C3 (13%) and C5 (12%) represent continental air masses coming from the south (south of France and Europe) and eastern side of Europe (mainly affected by the industrialized areas in NW and central Germany as well as Belgium), respectively.

The chemical composition of the aerosol particles as well as the contribution of OA factors were averaged over the different air mass

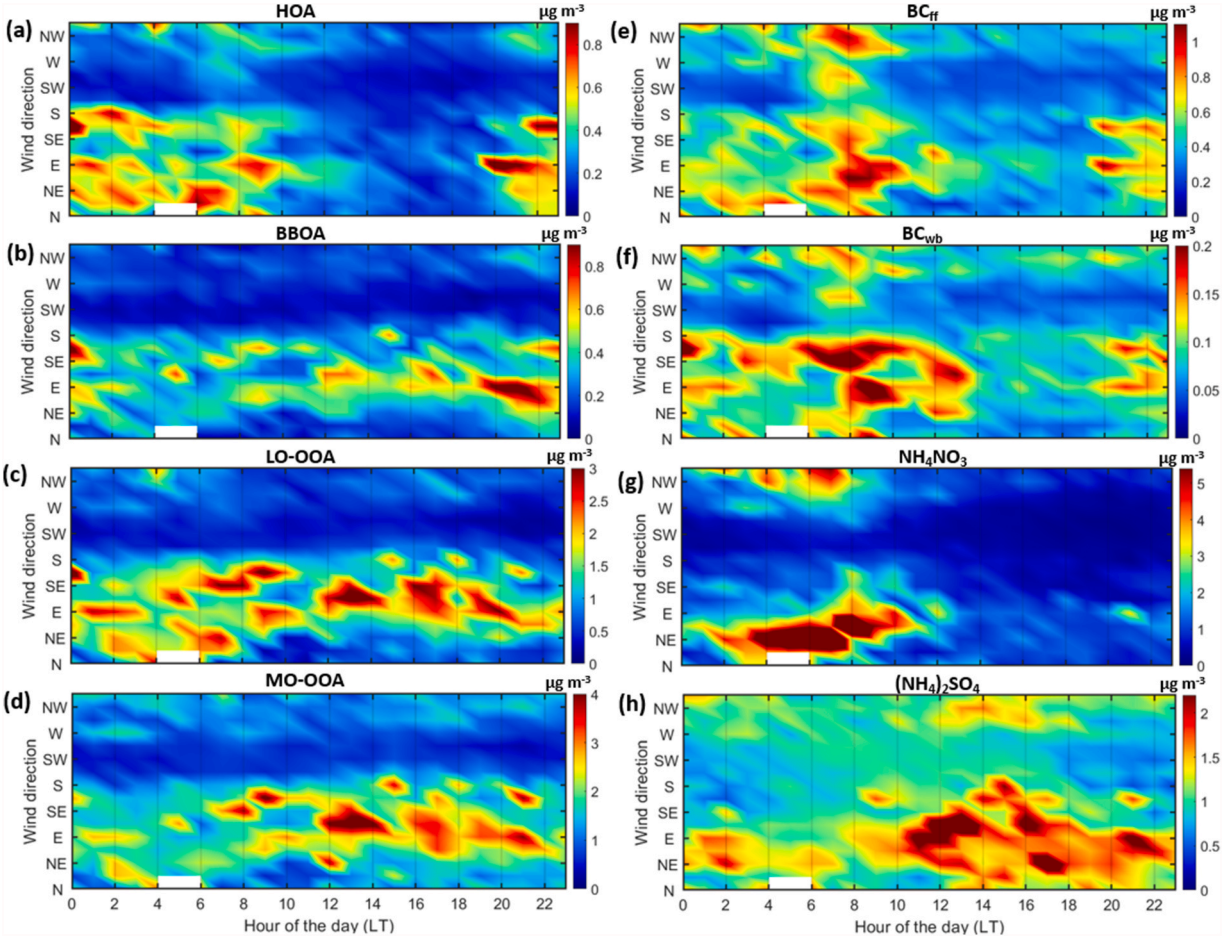

Fig. 6. Diel plots according to wind sectors during summertime for a) HOA, b) BBOA, c) LO-OOA, d) MO-OOA, e) BC_{ff}, f) BC_{wb}, g) NH_4NO_3, and h) $(NH_4)_2SO_4$. The Lille city center is located NW of the ATOLL site. The max value of the color scale represents the 90th percentile. (For interpretation of the references to color in this figure legend, the reader is referred to the Web version of this article.)

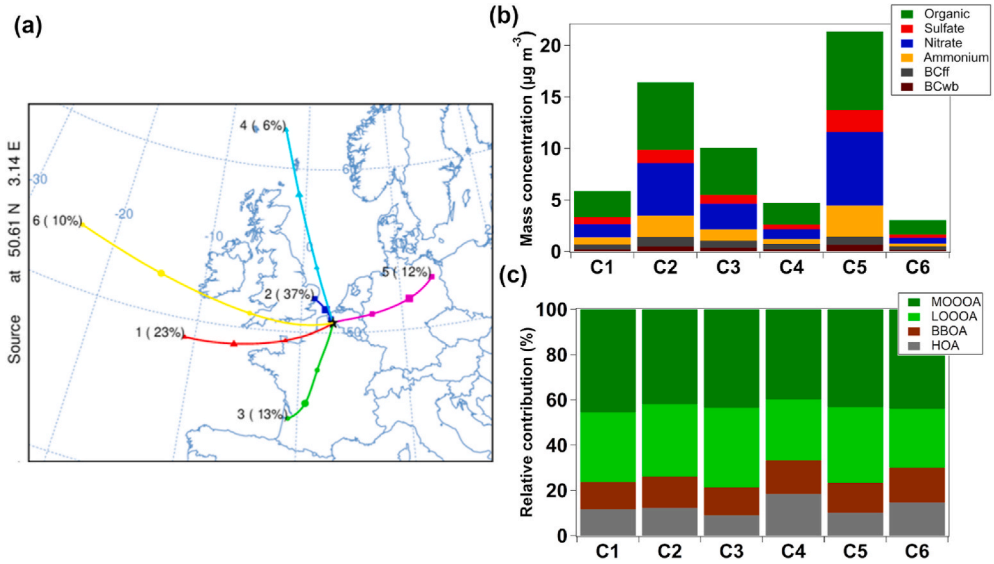

Fig. 7. Overview of the chemical composition and the OA factors for each cluster (C1 to C6), a) their trajectory map, b) the mean aerosol mass concentration associated with each cluster, and c) the relative contribution of the OA factors.

clusters and are presented in Fig. 7b and c. Overall, the highest particle mass concentrations were observed for clusters with the greatest continental influence (i.e., C3, south – 10.1 μg m^{-3}; C2, local – 16.5 μg m^{-3}; C5, east – 21.4 μg m^{-3}). The largest mass concentrations of nitrate, sulfate, and ammonium are also associated with these clusters, as well as a high contribution of LO-OOA and MO-OOA (more than 70%),

reflecting their regional origin or that of their gas-phase precursors. They are associated with the long-range transport of polluted continental air masses (C3 and C5) but are also related to local aged aerosol (C2). Those results are in line with receptor-based models and the chemistry-transport modeling applied by Potier et al. (2019), showing the important and frequent impact of "Near-East" areas (Belgium, Netherlands, Germany, etc.) on PM_{10} concentrations in the Northern France region. Meanwhile, the clusters C1, C4, and C6 with strong marine influence correspond to the lowest particle mass concentrations (C6, 3.0 μg $m^{-3;}$ C^4, 4.7 μg m^{-3}; C1, 5.9 μg m^{-3}) and they show a slight increase of POA PMF factor contributions (HOA and BBOA, 18.4% and 14.9% in C4, 14.6% and 15.5% in C6 respectively). These clusters are cleaner and mainly over water, thus HOA could be linked with shipping emissions over the Channel and North Sea, and northerly air masses with increased residential heating during wintertime. This analysis confirms the complex interaction between local and advected air masses on PM_1 concentrations and composition at the ATOLL platform.

4. Conclusion

Aerosol composition and sources in the newly established ATOLL site, near Lille in Northern France, are analyzed here from October 2016 to December 2020. During the studied period, PM_1 had a mean concentration of 10.6 μg m^{-3}, composed of OA (41.8%), NO_3 (28.9%), NH_4 (12.3%), SO_4 (8.6%), and BC (8.0%). For such a multi-annual dataset, source apportionment of organic aerosols has been performed using rolling PMF, allowing for a robust analysis through a clear set of criteria and constraints across seasons and years, in contrast to the season-by-season individual analysis method. A 28-day rolling PMF window shifted by one week over the four-year dataset yielded four factors, consisting of two primary OA, namely HOA (11.8% of total OA) mainly related to traffic, BBOA (ranging from 8.1% to 18.5% and peaking with the increase of residential heating in winter), and two oxygenated OA, LO-OOA (31.9%), and the MO-OOA (with a mean contribution of 42.3%). During wintertime, LO-OOA has been associated with aged biomass burning, identified recently as one of the key potential sources of negative health effects in Europe. Furthermore, the combined BBOA + LO-OOA attributes over 50% of OA to residential heating in winter at this site. Conversely, in summertime LO-OOA has been associated with biogenic SOA, also contributing significantly to OA (34.0%) during this season. The MO-OOA factor has been mostly linked with long-range transported air masses from continental areas. Pollution episodes are strongly linked with secondary processes. During summertime, LO-OOA increases with increasing PM_1 concentrations, linked with strong photochemical activity and high-temperature events, in agreement with enhanced new particle formation previously observed at this site and the expected SOA formation from increased emissions. In winter, spring, and autumn, ammonium nitrate, combined with oxidized organic aerosols (LO-OOA and MO-OOA) are key components during particulate pollution. Wind and trajectory analysis have shown a small impact of local pollution (Lille city) on the sampling site compared to the high regional impact. Overall, this study elucidates the main sources of fine aerosols at the ATOLL platform in Lille, describing the complex interactions between regional traffic, wood burning, agricultural activities, biogenic emissions, and long-range transport in this highly urbanized region of north-western Europe, towards developing effective mitigation policies. While exhaust traffic contribution to PM is expected to decrease in the coming years, wood burning (local and advected) will likely remain an important source of carbonaceous aerosols in Europe. Decreasing these primary sources could therefore lead to a decrease of both co-emitted precursor gases such as NOx and of secondary organic aerosols formed from anthropogenic precursors.

Author contributions

Hasna Chebaicheb: Data curation; Investigation; Methodology; Visualization; Writing – original draft. Joel F. de Brito: Supervision; Validation; Writing – original draft. Gang Chen: Methodology; Writing - review & editing. Emmanuel Tison: Data curation. Caroline Marchand: Supervision; Writing - review &editing. André S. H. Prévôt: Writing - review & editing. Olivier Favez: Supervision; Validation; Funding acquisition; Writing - review & editing.Véronique Riffault: Data curation; Validation; Funding acquisition; Supervision; Writing - review &editing.

Funding

H. Chebaicheb's PhD grant is supported by the LCSQA funded by the French Ministry of Environment. IMT Nord Europe acknowledges financial support from the Labex CaPPA project, which is funded by the French National Research Agency (ANR) through the PIA (Programme d'Investissement d'Avenir) under contract ANR-11-LABX-0005-01, and the CLIMIBIO and ECRIN projects, both financed by the Regional Council "Hauts-de-France" and the European Regional Development Fund (ERDF). IMT Nord Europe and INERIS participated in the COST COLOSSAL Action CA16109. The ATOLL site is one of the French ACTRIS National Facilities and contributes to the CARA program of the LCSQA funded by the French Ministry of Environment.

Declaration of competing interest

The authors declare that they have no known competing financial interests or personal relationships that could have appeared to influence the work reported in this paper.

Data availability

The data is freely available at the ACTRIS database (http://ebas-data.nilu.no/)

Acknowledgments

The authors are grateful to the staff at LOA, in particular Prof. P. Goloub, F. Auriol, and R. De Filippi, for supporting the technical and logistical implementation of the instruments, and to Dr. L.-H. Rivellini (now at the University of Toronto) for her early involvement. We thank T. Podvin (LOA) for providing the weather data at ATOLL, and the air quality monitoring network Atmo Hauts-de-France for providing $PM_{2.5}$ concentrations at the Lille Fives monitoring station.

Appendix A. Supplementary data

Supplementary data to this article can be found online at https://doi.org/10.1016/j.envpol.2023.121805.

References

Air quality in Europe 2021, 2021. European Environment Agency. URL. https://www.eea.europa.eu/publications/air-quality-in-europe-2021.

Allan, J.D., Jimenez, J.L., Williams, P.I., Alfarra, M.R., Bower, K.N., Jayne, J.T., Coe, H., Worsnop, D.R., 2003. Quantitative sampling using an Aerodyne aerosol mass spectrometer 1. Techniques of data interpretation and error analysis. J. Geophys. Res. Atmos. 108 https://doi.org/10.1029/2002JD002358.

Atabakhsh, S., Poulain, L., Chen, G., Canonaco, F., Prévôt, A.S.H., Pöhlker, M., Wiedensohler, A., Herrmann, H., 2023. A one-year ACSM source analysis of organic aerosol particle contributions from anthropogenic sources after long-range transport at the TROPOS research station Melpitz. Atmos. Chem. Phys. Discuss. 1–42. https://doi.org/10.5194/acp-2022-842.

Bressi, M., Cavalli, F., Putaud, J.P., Fröhlich, R., Petit, J.-E., Aas, W., Äijälä, M., Alastuey, A., Allan, J.D., Aurela, M., Berico, M., Bougiatioti, A., Bukowiecki, N., Canonaco, F., Crenn, V., Dusanter, S., Ehn, M., Elsasser, M., Flentje, H., Graf, P., Green, D.C., Heikkinen, L., Hermann, H., Holzinger, R., Hueglin, C., Keernik, H., Kiendler-Scharr, A., Kubelová, L., Lunder, C., Maasikmets, M., Makeš, O., Malaguti, A., Mihalopoulos, N., Nicolas, J.B., O'Dowd, C., Ovadnevaite, J., Petralia, E., Poulain, L., Priestman, M., Riffault, V., Ripoll, A., Schlag, P., Schwarz, J., Sciare, J., Slowik, J., Sosedova, Y., Stavroulas, I., Teinemaa, E., Via, M., Vodička, P.,

Williams, P.I., Wiedensohler, A., Young, D.E., Zhang, S., Favez, O., Minguillón, M.C., Prevot, A.S.H., 2021. A European aerosol phenomenology - 7: high-time resolution chemical characteristics of submicron particulate matter across Europe. Atmos. Environ. X 10, 100108. https://doi.org/10.1016/j.aeaoa.2021.100108.

Canonaco, F., Slowik, J.G., Baltensperger, U., Prévôt, A.S.H., 2015. Seasonal differences in oxygenated organic aerosol composition: implications for emissions sources and factor analysis. Atmos. Chem. Phys. 15, 6993–7002. https://doi.org/10.5194/acp-15-6993-2015.

Canonaco, F., Tobler, A., Chen, G., Sosedova, Y., Slowik, J.G., Bozzetti, C., Daellenbach, K.R., El Haddad, I., Crippa, M., Huang, R.-J., Furger, M., Baltensperger, U., Prévôt, A.S.H., 2021. A new method for long-term source apportionment with time-dependent factor profiles and uncertainty assessment using SoFi Pro: application to 1 year of organic aerosol data. Atmos. Meas. Tech. 14, 923–943. https://doi.org/10.5194/amt-14-923-2021.

Chazeau, B., Temime-Roussel, B., Gille, G., Mesbah, B., D'Anna, B., Wortham, H., Marchand, N., 2021. Measurement report: fourteen months of real-time characterisation of the submicronic aerosol and its atmospheric dynamics at the Marseille–Longchamp supersite. Atmos. Chem. Phys. 21, 7293–7319. https://doi.org/10.5194/acp-21-7293-2021.

Chen, G., Canonaco, F., Tobler, A., Aas, W., Alastuey, A., Allan, J., Atabakhsh, S., Aurela, M., Baltensperger, U., Bougiatioti, A., De Brito, J.F., Ceburnis, D., Chazeau, B., Chebaicheb, H., Daellenbach, K.R., Ehn, M., El Haddad, I., Eleftheriadis, K., Favez, O., Flentje, H., Font, A., Fossum, K., Freney, E., Gini, M., Green, D.C., Heikkinen, L., Herrmann, H., Kalogridis, A.-C., Keernik, H., Lhotka, R., Lin, C., Lunder, C., Maasikmets, M., Manousakas, M.I., Marchand, N., Marin, C., Marmureanu, L., Mihalopoulos, N., Močnik, G., Nęcki, J., O'Dowd, C., Ovadnevaite, J., Peter, T., Petit, J.-E., Pikridas, M., Matthew Platt, S., Pokorná, P., Poulain, L., Priestman, M., Riffault, V., Rinaldi, M., Różański, K., Schwarz, J., Sciare, J., Simon, L., Skiba, A., Slowik, J.G., Sosedova, Y., Stavroulas, I., Styszko, K., Teinemaa, E., Timonen, H., Tremper, A., Vasilescu, J., Via, M., Vodička, P., Wiedensohler, A., Zografou, O., Cruz Minguillón, M., Prévôt, A.S.H., 2022. European aerosol phenomenology − 8: harmonised source apportionment of organic aerosol using 22 Year-long ACSM/AMS datasets. Environ. Int. 166, 107325 https://doi.org/10.1016/j.envint.2022.107325.

Chen, G., Sosedova, Y., Canonaco, F., Fröhlich, R., Tobler, A., Vlachou, A., Daellenbach, K.R., Bozzetti, C., Hueglin, C., Graf, P., Baltensperger, U., Slowik, J.G., El Haddad, I., Prévôt, A.S.H., 2021. Time-dependent source apportionment of submicron organic aerosol for a rural site in an alpine valley using a rolling positive matrix factorisation (PMF) window. Atmos. Chem. Phys. 21, 15081–15101. https://doi.org/10.5194/acp-21-15081-2021.

Crenn, V., Fronval, I., Petitprez, D., Riffault, V., 2017. Fine particles sampled at an urban background site and an industrialized coastal site in Northern France - Part 1: seasonal variations and chemical characterization. Sci. Total Environ. 578, 203–218.

Crippa, M., Canonaco, F., Lanz, V.A., Äijälä, M., Allan, J.D., Carbone, S., Capes, G., Ceburnis, D., Dall'Osto, M., Day, D.A., DeCarlo, P.F., Ehn, M., Eriksson, A., Freney, E., Hildebrandt Ruiz, L., Hillamo, R., Jimenez, J.L., Junninen, H., Kiendler-Scharr, A., Kortelainen, A.-M., Kulmala, M., Laaksonen, A., Mensah, A.A., Mohr, C., Nemitz, E., O'Dowd, C., Ovadnevaite, J., Pandis, S.N., Petäjä, T., Poulain, L., Saarikoski, S., Sellegri, K., Swietlicki, E., Tiitta, P., Worsnop, D.R., Baltensperger, U., Prévôt, A.S.H., 2014. Organic aerosol components derived from 25 AMS data sets across Europe using a consistent ME-2 based source apportionment approach. Atmos. Chem. Phys. 14, 6159–6176. https://doi.org/10.5194/acp-14-6159-2014.

Crumeyrolle, S., Kontkanen, J.S.S., Rose, C., Velazquez Garcia, A., Bourrianne, E., Catalfamo, M., Riffault, V., Tison, E., Ferreira de Brito, J., Visez, N., Ferlay, N., Auriol, F., Chiapello, I., 2023. Measurement report: atmospheric new particle formation at a peri-urban site in Lille, northern France. Atmos. Chem. Phys. 23, 183–201. https://doi.org/10.5194/acp-23-183-2023.

Daellenbach, K.R., Uzu, G., Jiang, J., Cassagnes, L.-E., Leni, Z., Vlachou, A., Stefenelli, G., Canonaco, F., Weber, S., Segers, A., Kuenen, J.J.P., Schaap, M., Favez, O., Albinet, A., Aksoyoglu, S., Dommen, J., Baltensperger, U., Geiser, M., El Haddad, I., Jaffrezo, J.-L., Prévôt, A.S.H., 2020. Sources of particulate-matter air pollution and its oxidative potential in Europe. Nature 587, 414–419. https://doi.org/10.1038/s41586-020-2902-8.

Draxler, RR, 1999. HYSPLIT4 users's guide.

Drinovec, L., Močnik, G., Zotter, P., Prévôt, A.S.H., Ruckstuhl, C., Coz, E., Rupakheti, M., Sciare, J., Müller, T., Wiedensohler, A., Hansen, A.D.A., 2015. The "dual-spot" Aethalometer: an improved measurement of aerosol black carbon with real-time loading compensation. Atmos. Meas. Tech. 8, 1965–1979. https://doi.org/10.5194/amt-8-1965-2015.

Efron, B., 1979. Bootstrap methods: another look at the jackknife. Ann. Stat. 7, 1–26. https://doi.org/10.1214/aos/1176344552.

Favez, O., Weber, S., Petit, J.-E., Alleman, L., Albinet, A., Riffault, V., Chazeau, B., Amodeo, T., Salameh, D., Zhang, Y., Srivastava, D., Samaké, A., Aujay, R., Papin, A., Bonnaire, N., Boullanger, C., Chatain, M., Chevrier, F., Detournay, A., Leoz-Garziandia, E., 2021. Overview of the French Operational Network for in Situ Observation of PM Chemical Composition and Sources in Urban Unvironments (CARA Program). https://doi.org/10.20944/preprints202101.0182.v1.

Hendriks, C., Kranenburg, R., Kuenen, J.J.P., Van den Bril, B., Verguts, V., Schaap, M., 2016. Ammonia emission time profiles based on manure transport data improve ammonia modelling across north western Europe. Atmos. Environ. 131, 83–96. https://doi.org/10.1016/j.atmosenv.2016.01.043.

Hu, W.W., Campuzano-Jost, P., Palm, B.B., Day, D.A., Ortega, A.M., Hayes, P.L., Krechmer, J.E., Chen, Q., Kuwata, M., Liu, Y.J., de Sá, S.S., McKinney, K., Martin, S. T., Hu, M., Budisulistiorini, S.H., Riva, M., Surratt, J.D., Clair J M, St, Isaacman-Van Wertz, G., Yee, L.D., Goldstein, A.H., Carbone, S., Brito, J., Artaxo, P., de Gouw, J.A., Koss, A., Wisthaler, A., Mikoviny, T., Karl, T., Kaser, L., Jud, W., Hansel, A., Docherty, K.S., Alexander, M.L., Robinson, N.H., Coe, H., Allan, J.D., Canagaratna, M.R., Paulot, F., Jimenez, J.L., 2015. Characterization of a real-time tracer for isoprene epoxydiols-derived secondary organic aerosol (IEPOX-SOA) from aerosol mass spectrometer measurements. Atmos. Chem. Phys. 15, 11807–11833. https://doi.org/10.5194/acp-15-11807-2015.

Kelly, F.J., Fussell, J.C., 2015. Air pollution and public health: emerging hazards and improved understanding of risk. Environ. Geochem. Health 37, 631–649. https://doi.org/10.1007/s10653-015-9720-1.

Middlebrook, A.M., Bahreini, R., Jimenez, J.L., Canagaratna, M.R., 2012. Evaluation of composition-dependent collection efficiencies for the Aerodyne aerosol mass spectrometer using field data. Aerosol Sci. Technol. 46, 258–271. https://doi.org/10.1080/02786826.2011.620041.

Ng, N.L., Canagaratna, M.R., Jimenez, J.L., Zhang, Q., Ulbrich, I.M., Worsnop, D.R., 2011a. Real-time methods for estimating organic component mass concentrations from aerosol mass spectrometer data. Environ. Sci. Technol. 45, 910–916. https://doi.org/10.1021/es102951k.

Ng, N.L., Herndon, S.C., Trimborn, A., Canagaratna, M.R., Croteau, P.L., Onasch, T.B., Sueper, D., Worsnop, D.R., Zhang, Q., Sun, Y.L., Jayne, J.T., 2011b. An aerosol chemical speciation monitor (ACSM) for routine monitoring of the composition and mass concentrations of ambient aerosol. Aerosol Sci. Technol. 45, 780–794. https://doi.org/10.1080/02786826.2011.560211.

Paatero, P., Tapper, U., 1994. Positive matrix factorization: a non-negative factor model with optimal utilization of error estimates of data values. Environmetrics 5, 111–126. https://doi.org/10.1002/env.3170050203.

Pandis, S.N., Skyllakou, K., Florou, K., Kostenidou, E., Kaltsonoudis, C., Hasa, E., Presto, A.A., 2016. Urban particulate matter pollution: a tale of five cities. Faraday Discuss 189, 277–290. https://doi.org/10.1039/C5FD00212E.

Parworth, C., Fast, J., Mei, F., Shippert, T., Sivaraman, C., Tilp, A., Watson, T., Zhang, Q., 2015. Long-term measurements of submicrometer aerosol chemistry at the southern great plains (SGP) using an aerosol chemical speciation monitor (ACSM). Atmos. Environ. 106, 43–55. https://doi.org/10.1016/j.atmosenv.2015.01.060.

Petit, J.-E., Favez, O., Sciare, J., Crenn, V., Sarda-Estève, R., Bonnaire, N., Močnik, G., Dupont, J.-C., Haeffelin, M., Leoz-Garziandia, E., 2015. Two years of near real-time chemical composition of submicron aerosols in the region of Paris using an Aerosol Chemical Speciation Monitor (ACSM) and a multi-wavelength Aethalometer. Atmos. Chem. Phys. 15, 2985–3005. https://doi.org/10.5194/acp-15-2985-2015.

Potier, E., Waked, A., Bourin, A., Minvielle, F., Péré, J.C., Perdrix, E., Michoud, V., Riffault, V., Alleman, L.Y., Sauvage, S., 2019. Characterizing the regional contribution to PM10 pollution over northern France using two complementary approaches: chemistry transport and trajectory-based receptor models. Atmos. Res. 223, 1–14. https://doi.org/10.1016/j.atmosres.2019.03.002.

Roig Rodelas, R., Perdrix, E., Herbin, B., Riffault, V., 2019. Characterization and variability of inorganic aerosols and their gaseous precursors at a suburban site in northern France over one year (2015–2016). Atmos. Environ. 200, 142–157. https://doi.org/10.1016/j.atmosenv.2018.11.041.

Sandradewi, J., Prévôt, A.S.H., Szidat, S., Perron, N., Alfarra, M.R., Lanz, V.A., Weingartner, E., Baltensperger, U., 2008. Using aerosol light absorption measurements for the quantitative determination of wood burning and traffic emission contributions to particulate matter. Environ. Sci. Technol. 42, 3316–3323. https://doi.org/10.1021/es702253m.

Schlag, P., Kiendler-Scharr, A., Blom, M.J., Canonaco, F., Henzing, J.S., Moerman, M., Prévôt, A.S.H., Holzinger, R., 2016. Aerosol source apportionment from 1-year measurements at the CESAR tower in Cabauw, The Netherlands. Atmos. Chem. Phys. 16, 8831–8847. https://doi.org/10.5194/acp-16-8831-2016.

Thunis, P., Pisoni, E., Bessagnet, B., Wilson, J., Vignati, E., De Meij, A., Mascherpa, A., 2021. Urban PM2.5 Atlas [WWW Document]. JRC Publ. Repos. https://doi.org/10.2760/356670.

Tobler, A.K., Skiba, A., Canonaco, F., Močnik, G., Rai, P., Chen, G., Bartyzel, J., Zimnoch, M., Styszko, K., Nęcki, J., Furger, M., Różański, K., Baltensperger, U., Slowik, J.G., Prevot, A.S.H., 2021. Characterization of non-refractory (NR) PM_1 and source apportionment of organic aerosol in Kraków, Poland. Atmos. Chem. Phys. 21, 14893–14906. https://doi.org/10.5194/acp-21-14893-2021.

Velazquez-Garcia, A., Crumeyrolle, S., de Brito, J.F., Tison, E., Bourrianne, E., Chiapello, I., Riffault, V., 2023. Deriving composition-dependent aerosol absorption, scattering and extinction mass efficiencies from multi-annual high time resolution observations in Northern France. Atmos. Environ., 119613 https://doi.org/10.1016/j.atmosenv.2023.119613.

Via, M., Minguillón, M.C., Reche, C., Querol, X., Alastuey, A., 2021. Increase in secondary organic aerosol in an urban environment. Atmos. Chem. Phys. 21, 8323–8339. https://doi.org/10.5194/acp-21-8323-2021.

Waked, A., Bourin, A., Michoud, V., Perdrix, E., Alleman, L.Y., Sauvage, S., Delaunay, T., Vermeesch, S., Petit, J.-E., Riffault, V., 2018. Investigation of the geographical origins of PM10 based on long, medium and short-range air mass back-trajectories impacting Northern France during the period 2009–2013. Atmos. Environ. 193, 143–152. https://doi.org/10.1016/j.atmosenv.2018.08.015.

Waked, A., Favez, O., Alleman, L.Y., Piot, C., Petit, J.-E., Delaunay, T., Verlinden, E., Golly, B., Besombes, J.-L., Jaffrezo, J.-L., Leoz-Garziandia, E., 2014. Source apportionment of PM_{10} in a north-western Europe regional urban background site (Lens, France) using positive matrix factorization and including primary biogenic emissions. Atmos. Chem. Phys. 14, 3325–3346. https://doi.org/10.5194/acp-14-3325-2014.

WHO Air Quality Guidelines, 2021. URL https://www.c40knowledgehub.org/s/article/WHO-Air-Quality-Guidelines?language=en_US (accessed January.23.23).

Zhang, Y., Favez, O., Petit, J.-E., Canonaco, F., Truong, F., Bonnaire, N., Crenn, V., Amodeo, T., Prévôt, A.S.H., Sciare, J., Gros, V., Albinet, A., 2019. Six-year source apportionment of submicron organic aerosols from near-continuous highly time-

resolved measurements at SIRTA (Paris area, France). Atmos. Chem. Phys. 19, 14755–14776. https://doi.org/10.5194/acp-19-14755-2019.

Zhang, S., Tison, E., Dusanter, S., Beaugard, C., Gengembre, C., Augustin, P., Fourmentin, M., Delbarre, H., Riffault, V., 2021. Near real-time PM1 chemical composition measurements at a French urban background and coastal site under industrial influence over more than a year: Temporal variability and assessment of sulfur-containing emissions. Atmos. Environ. 244, 117960. https://doi.org/10.1016/j.atmosenv.2020.117960.

Zografou, O., Gini, M., Manousakas, M.I., Chen, G., Kalogridis, A.C., Diapouli, E., Pappa, A., Eleftheriadis, K., 2022. Combined organic and inorganic source apportionment on yearlong ToF-ACSM dataset at a suburban station in Athens, Atmospheric Meas. Technol. 15, 4675–4692. https://doi.org/10.5194/amt-15-4675-2022.